

---

This manuscript is a *preprint* that has been accepted for publication in *The Sedimentary Record*. It has been peer-reviewed but has not undergone copyediting and typesetting. Upon publication, the final version of this manuscript will be linked via DOI in the description.

---

5<sup>th</sup> May, 2024

1 **TITLE: THE FATE OF BARS IN BRAIDED RIVERS**

2 Authors: Alpheus, S.<sup>1</sup> & Hajek, E.<sup>1</sup>

3 Author affiliations: 1- Department of Geosciences, The Pennsylvania State University, University Park,

4 PA 16802

5 *Keywords: stratigraphic architecture; braided rivers; channel threads; bar; braid bar; confluence, fluvial*

6 *sedimentology*

7

8 **ABSTRACT**

9 Ancient river deposits are important archives of past landscape conditions on planetary surfaces.  
10 On Earth, they host valuable groundwater, energy resources, and carbon-storage potential. Reconstructing  
11 details of paleochannel forms and movements refines our understanding of the controls on river behavior  
12 under different climate, landcover, and tectonic conditions, and improves predictions and models of  
13 subsurface reservoirs. While studies have shown detailed connections between channel kinematics and bar-  
14 deposit architecture in meandering river systems, similar connections between braided river movements and  
15 preserved braided river deposits have not been established. Here we explore the potential for connecting  
16 braided river deposits to paleochannel movements, form, and flow conditions, and we evaluate the controls  
17 on bar preservation using synthetic stratigraphy generated with a numerical morphodynamic model. We  
18 investigate how attributes of channel morphodynamics, like channel widening or braiding intensity, impact  
19 bar deposits' preservation, scale, geometry, and architecture. We then assess how the scale, preservation,  
20 and facies composition of bar deposits reflect formative flow conditions of the channel. Our results  
21 demonstrate that no diagnostic signature of braided channel morphodynamics is recorded in bar-deposit  
22 geometry, facies, or preservation patterns. Rather, the unique local history of thread movements combines  
23 stochastically to preserve or rework bar deposits, and the timing of channel avulsion is the dominant control  
24 on bar preservation. Our results also show that representative paleochannel flow conditions will likely be  
25 accurately reflected in aggregate observations of braid bar deposits within channel-belt sandbodies at a  
26 regional or member/formation scale. These results demonstrate the need for broad sampling and statistical  
27 approaches to subsurface prediction and paleo-flow reconstruction in ancient, braided river deposits.

28

29

30

## 31 INTRODUCTION

32 Ancient channel deposits are important archives of past landscape conditions on planetary surfaces.  
33 Reconstructing paleoflow conditions and paleochannel kinematics from river deposits provides  
34 opportunities to constrain ancient landscape conditions (e.g., Holbrook and Wanas, 2014; Lyster et al.,  
35 2021, 2022; Hartley and Owen, 2022; Wood et al., 2023; McLeod et al., 2023); understand river response  
36 to changes in climate, tectonics, and land cover (e.g., Foreman et al., 2012; Foreman, 2014; McMahon and  
37 Davies, 2018; Barefoot et al., 2022; Ielpi et al., 2022; Sharma et al., 2023); and predict the distribution and  
38 migration of subsurface fluids in alluvial basins (e.g., Bridge and Lunt, 2006; Lewis et al., 2018; Martin et  
39 al., 2021; Guo et al., 2022). Details about paleochannel movements are recorded in the geometry,  
40 arrangement and preservation character of bar deposits in ancient channel fills (e.g., Colombera et al., 2017;  
41 Durkin et al., 2017, 2018; Chamberlin and Hajek, 2019) and are useful in answering outstanding questions  
42 about channel mobility (e.g. Mohrig et al., 2000; Wickert et al., 2013; Sahoo et al., 2020), channel planform  
43 (e.g., Gibling, 2006; Hartley et al., 2015), and river response to flow variability (e.g., Sambrook Smith et  
44 al., 2010; Nicholas et al., 2016; Li et al., 2023). Additionally, the height of fully preserved clinofolds  
45 (Figure 1) is a proxy for paleo-flow depth (Mohrig et al., 2000; Hajek and Heller, 2012)—an essential  
46 parameter in reconstructing the paleohydraulic conditions of ancient rivers (e.g., Hartley et al., 2015;  
47 Mahon and McElroy, 2018; Lyster et al., 2021, 2022; Hartley and Owen, 2022). To this end,  
48 understanding the controls on channel-bar preservation is critical for accurately reconstructing and  
49 comparing the behavior and response of ancient rivers to different land cover, climate, and tectonic  
50 conditions.

51 Preservation of features like bedforms, barforms, and channels in fluvial deposits has been explored  
52 at a variety of scales in field, experimental, and numerical systems (e.g., Leclair et al., 1997; Ganti et al.,  
53 2013; Reesink et al., 2015; van de Lageweg et al., 2016b; Fielding et al., 2018; Chamberlin and Hajek,  
54 2019; Leary and Ganti, 2020; Das et al., 2022). Previous theoretical, experimental, and numerical studies

55 have shown relationships between bedform height and the distribution of cross-set thicknesses (e.g., Paola  
56 and Borgman, 1991; Bridge, 1997; Leclair et al., 1997; Jerolmack and Mohrig, 2005; Ganti et al., 2013;  
57 Bradley and Venditti, 2017). At the bar scale, flow conditions and hierarchies of bed features (e.g., bedforms  
58 and bars) impact the relationship between preserved cross-strata and formative topography (e.g., Nicholas  
59 et al., 2016; Sambrook Smith et al., 2019; Ganti et al., 2020). At the largest scale in river networks, the  
60 frequency of channel avulsion and the nature of sediment supply to basins impacts channel-belt preservation  
61 and amalgamation (e.g., Heller and Paola, 1996; Strong et al., 2005; Chamberlin and Hajek, 2019;  
62 Chadwick et al., 2022; Cardenas et al., 2023).

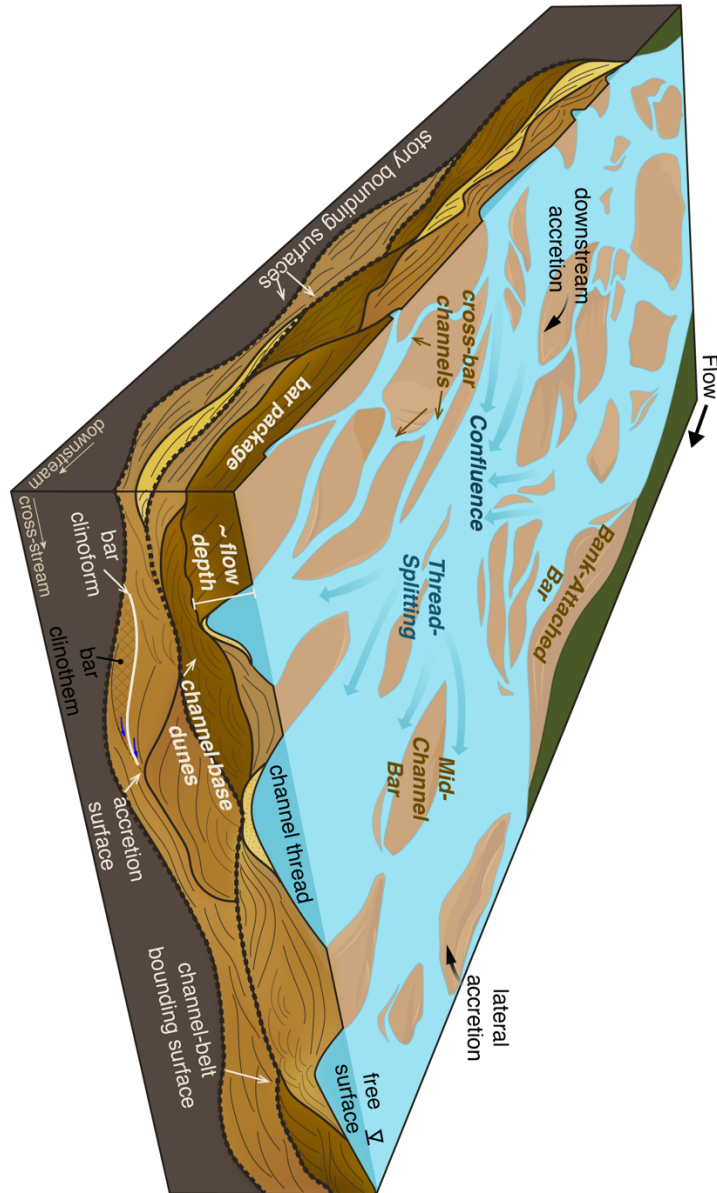
63         Controls on the preservation of bar-scale deposits remain poorly understood for braided rivers. Bars  
64 are not explicitly captured at the experimental scales used to test theoretical and conceptual models about  
65 controls on bed-scale (e.g., Ganti et al., 2013; Leary and Ganti, 2020; Bradley and Venditti, 2021; Das et  
66 al., 2022) or landscape/channel-belt scale preservation (e.g., Heller and Paola, 1996; Martin et al., 2009;  
67 Paola et al., 2009; Straub and Wang, 2013; Chamberlin and Hajek, 2015, 2019). Consequently, bar  
68 preservation is studied using field observations and remote imagery of modern systems (e.g., Dixon et al.,  
69 2018; Chamberlin and Hajek, 2019; Cardenas et al., 2020; Rahman, 2023) and numerical models (e.g.,  
70 Kleinhans and van den Berg, 2011; Schuurman and Kleinhans, 2015; Nicholas et al., 2016; van de Lageweg  
71 et al., 2016b, 2016a; Sambrook Smith et al., 2019; Li et al., 2023). These investigations have shown that  
72 channel-thread kinematics such as lateral migration, widening, thread-splitting, and confluence, influence  
73 the formation and morphology of bars in braided rivers (Figure 1). Furthermore, perturbations in flow and  
74 sediment supply across multiple scales (e.g., local-, reach-, and system-scale) can influence thread position  
75 and mobility, affecting the configuration and kinematics of channel threads and bars in braided rivers. This  
76 has been observed in systems where migrating and deforming bars and migrating threads alter local flow  
77 paths and network configurations (e.g., Wintenberger et al., 2015; Schuurman et al., 2016; Dixon et al.,  
78 2018; Le Guern et al., 2023), or where the configuration and migration behavior of bars and threads in

79 braided networks is altered in response to flooding events and land-use change (e.g., Jarriel et al., 2021;  
80 Tejedor et al., 2022; Ghosh et al., 2023).

81           Despite careful work connecting braided river morphodynamics to bar morphology and migration  
82 (e.g., Germanoski and Schumm, 1993; Lunt et al., 2004; Ashworth et al., 2011; Schuurman and Kleinhans,  
83 2015; Fielding, 2022) and detailed descriptions of ancient deposits (e.g., Miall, 1988; Bridge, 1993; Lunt  
84 et al., 2004; Bridge and Lunt, 2006; Fielding et al., 2018; Chamberlin and Hajek, 2019; Cardenas et al.,  
85 2020; Barefoot et al., 2022), specific connections between braided river kinematics and bar deposit  
86 preservation are lacking. Facies models suggest that braided river deposits are dominated by laterally  
87 extensive and amalgamated sand bodies that comprise multiple bar deposits, channel floor cross-strata and  
88 occasional pockets of low-flow or abandonment fines (Miall, 1985, 1988; Gibling, 2006; Lynds and Hajek,  
89 2006; Hajek et al., 2010; Ashworth et al., 2011). The high degree of channel mobility in braided rivers  
90 suggests that their deposits should be reworked, with common, truncated bar packages and amalgamated  
91 channel bodies (e.g., Best et al., 2003; Bridge and Lunt, 2006; Gibling, 2006; Ashworth et al., 2011;  
92 Wickert et al., 2013). In meandering systems, the geometry, preservation, and facies of point bar deposits  
93 can reflect specific channel kinematics changing bend curvature, translation, or rotation, and chute or neck  
94 cutoffs, (e.g., Smith et al., 2011; Durkin et al., 2017, 2018; Sylvester et al., 2021). In braided rivers, thread  
95 migration and bifurcation have been observed to result in bar accretion, translation, deformation, and  
96 migration (e.g., Rice et al., 2009; Schuurman et al., 2013; Sambrook Smith et al., 2019). However, it is  
97 unclear whether braid bar preservation reflects specific channel movements, as shown for meandering  
98 systems. Additionally, the role of these movements in controlling channel-belt facies distribution in braided  
99 river deposits has not been fully explored. Deepening our understanding of the controls on braid bar  
100 preservation and stratigraphic architecture will improve our ability to generate nuanced facies models,  
101 compare modern, ancient, and model systems, and assess uncertainties associated with paleo-

102 morphodynamic reconstructions (e.g., Holbrook and Wanas, 2014; Mahon and McElroy, 2018; Lyster et  
103 al., 2022)

104       Taken together, thread movements, channel kinematics, discharge variability, and intrinsic flow  
105 complexity in braided rivers impart stochasticity on bar formation, migration, and reworking. Here we  
106 explore the degree to which this stochasticity controls the fate of bars in braided rivers and our ability to  
107 reconstruct paleochannel conditions from ancient, braided river deposits. We used a physics-based  
108 morphodynamic model to investigate the baseline, autogenic statistics of bar preservation in a braided river  
109 under constant flow and sediment supply conditions. Using synthetic stratigraphy generated from the  
110 model, we evaluated how channel form and kinematics, including the degree of braiding and channel-belt  
111 widening, impact bar preservation. Using observations from synthetic stratigraphy that reflect field  
112 measurements obtainable from ancient outcrops, we identify field-scale observations and sampling  
113 strategies that can be particularly insightful for interpreting and reconstructing paleohydraulic conditions  
114 from ancient, braided river archives.



115

116 Figure 1: Conceptual diagram of a braided river and its stratigraphic deposits. Zones of thread confluence  
 117 and thread splitting, shown by blue arrows, facilitate the formation, accretion, and deformation of bank-  
 118 attached and mid-channel bars. Within a larger channel-belt sand body, bar deposits can be stratigraphically  
 119 preserved as packages characterized by sigmoidal bar clinothems that accrete in the direction of bar growth  
 120 and downlap (e.g., blue arrows in cross-stream stratigraphic view) onto older deposits.

## 121 METHODS

122 We simulated the formation and evolution of a braided river under constant flow conditions using  
123 the numerical model, NAYS2DH, which solves two-dimensional, depth-averaged momentum and  
124 continuity equations over an orthogonal, curvilinear grid to simulate channelized flow and river-bed  
125 deformation (Jang and Shimizu, 2005; Shimizu et al., 2011; Asahi et al., 2013; Nelson et al., 2016). While  
126 we were not simulating conditions of any specific rivers, the model parameters we used broadly capture the  
127 dynamics of mid-sized, sand-bedded braided rivers and generate stratigraphic cross-sections with  
128 geometries and architectures reflective of many well-studied braided river deposits (e.g., Castlegate  
129 Sandstone, Kayenta Formation, Salt Wash Member of the Morrison Formation (e.g., Miall, 1988; Miall,  
130 1994; Adams and Bhattacharya, 2005; McLaurin and Steel, 2007; Owen et al., 2015). The model was run  
131 over a 10 km long by 100 m wide initial grid with a slope of 0.001, and water discharge  $100 \text{ m}^3/\text{s}$  with  
132 random noise of up  $\pm 0.5 \text{ m}^3/\text{s}$  to maintain bar growth and decay. NAYS2DH is a transport-limited model  
133 in which sediment supply is determined by discharge (Shimizu et al., 2011); our model had a uniform  
134 sediment grain size of 0.31 mm. The model ran for 31.8 days with a morphodynamic scaling factor of 25,  
135 meaning the model simulated approximately 2.2 years (26 months) of activity output in 382 timesteps. It  
136 took the model 80 timesteps to reach a dynamic bed equilibrium (model spin-up time), and we ran the  
137 model for  $\sim 5$ x this initial bed equilibrium time. Our model run was spanned approximately 32 times the  
138 average bar turnover timescale (Myrow et al., 2018)—estimated as the amount of time required to displace  
139 a bar in the downstream direction based on the unit sediment flux (Figure S2)—sufficient to completely  
140 rework the entire model bed multiple times throughout the run. The studied reach (1000 m to 9000 m) in  
141 the model domain was approximately 150 times as long as the average bar length. Processes like thread  
142 splitting and confluence, bar deposition, and channel widening arise spontaneously in the model, and thread  
143 and bar positions evolve and shift in ways that mimic multi-thread systems like in the Brahmaputra-Jamuna  
144 (e.g., Dixon et al., 2018; Rahman, 2023), Loire (e.g., Wintenberger et al., 2015; Le Guern et al., 2023),

145 Sunwapta and South Saskatchewan rivers (e.g., Van Den Berg and Van Gelder, 1993) (Figure 2 Panel A).  
146 To end the run, we abruptly stopped the model simulating channel avulsion.

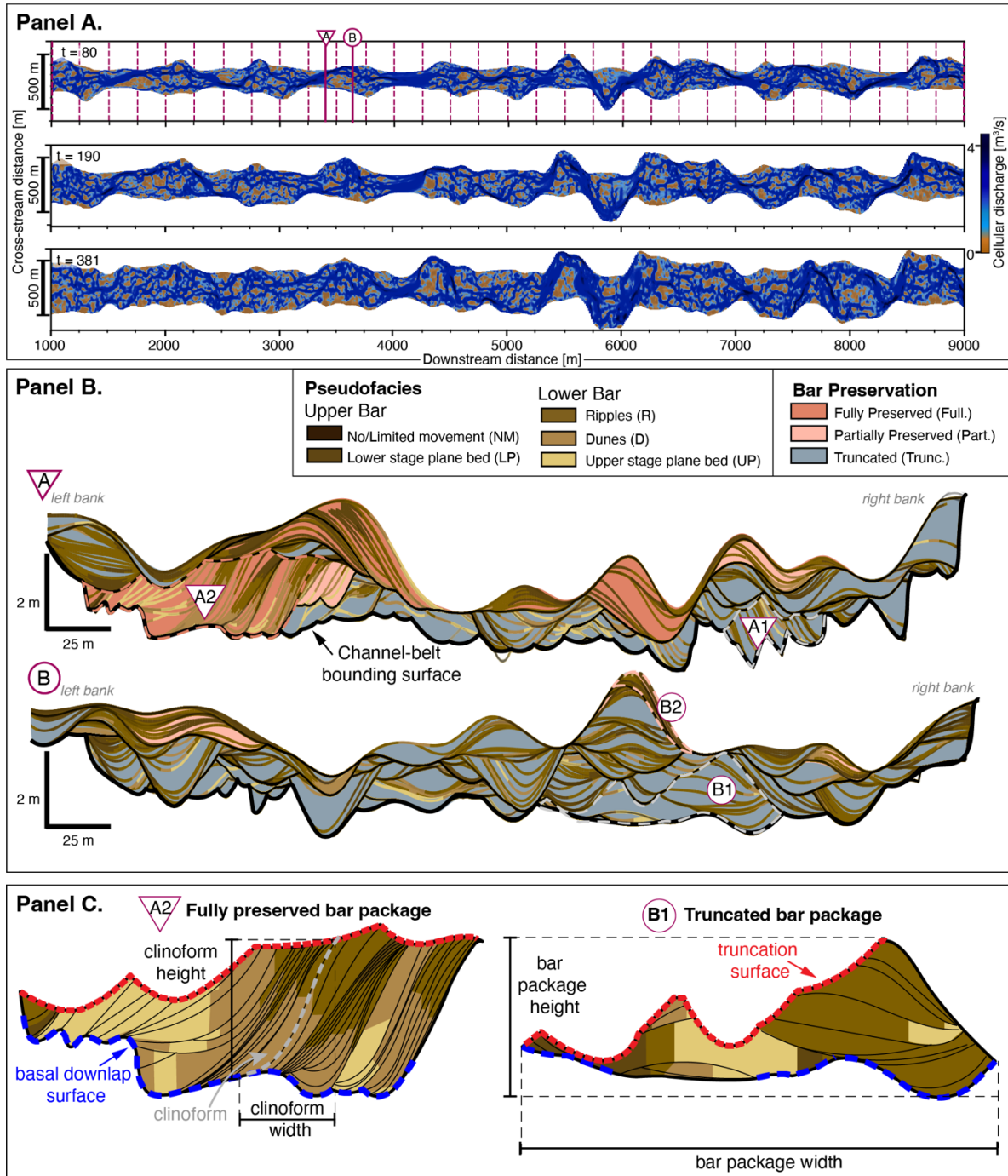
147 We built synthetic stratigraphic sections from the model by stacking channel-floor topography  
148 through time (Figure 2 Panel B). For each timestep at each bed location, we used local flow depth and  
149 velocity conditions to predict the stability of different bedforms (here referred to as '*pseudo-structures*')  
150 based on a representative experimental bedform-stability relationship (i.e. an example association between  
151 flow properties like shear stress, bed-material transport, and bed form) and the 0.31 mm grain size supplied  
152 in the model (Figure S1). We used these pseudo-structures to map bar facies onto these surfaces in the  
153 stratigraphic cross-sections (Figure 2 Panels B and C). Following the field-based mapping approach of  
154 Chamberlin and Hajek (2019), we defined lower bar facies as having higher-flow pseudo-structures like  
155 ripples, dunes and upper-stage plane bedding, and upper bar facies with lower-flow pseudo-structures such  
156 as lower-stage plane bedding and no movement. Bar-deposit packages were defined as conformable units  
157 of deposition bound by surfaces of non-deposition or erosion identified by downlap, onlap, offlap, and  
158 truncation stratal relationships (Figure 2 Panel C). We mapped bar packages in 33 cross-sections at a 250m  
159 spacing along the length of the model reach, excluding the first and last 1km stretches to avoid model—  
160 boundary effects.

161 For each bar package we characterized the degree of preservation using approaches previously used  
162 to classify bar preservation in ancient outcrops (Chamberlin and Hajek, 2019; Barefoot et al., 2022) where  
163 bar packages that contain both upper bar facies and bar-top rollover geometry are 'Fully Preserved' (Full.),  
164 packages with bar top rollover or upper bar facies are 'Partially Preserved' (Part.), and ones with neither  
165 upper-bar facies nor rollover are 'Truncated' (Trunc.) (Figure 2 Panels B and C). We measured the  
166 geometry (width, thickness, and area) and age of bar packages, and evaluated the deposition rate, and  
167 duration of deposition associated with each bar package. For each cross-section we compared bar-package  
168 preservation to aspects of braided network form and evolution including thread count, Entropic Braiding

169 Index (eBI, Tejedor et al., 2022), and widening rate, to explore how these kinematics influence bar  
170 preservation.

171

172



173

174 Figure 2: Braided river evolution and bar stratigraphic mapping from NAYS2DH morphodynamic model.

175 Panel A: Model bed evolution at three timesteps:  $t = 80$  (end-of model spin-up),  $t = 190$  (model midpoint)

176 and  $t = 381$  (abandonment/model termination). Pink dashed lines in the top snapshot ( $t = 80$ ) indicate

177 locations of cross-sections mapped in this study, and solid lines indicate locations of two example cross

178 sections: A (triangle) and B (circle) shown in panels below. The video of the complete model run is linked  
179 in the supplementary material. Panel B: Example model cross-sections A (triangle) and B (circle), fully  
180 mapped to illustrate bar packages, categorized by degree of bar preservation. Black lines outline bar-package  
181 bounding surfaces with internal bar surfaces (timelines) tracing bar evolution colored by modeled bar  
182 pseudo-structures assigned using relationships between bedform-stability and local flow conditions. Bar  
183 packages highlighted in Panel C and in Figure 5 are outlined with dashed lines (A1, A2, B1). Panel C:  
184 Example fully preserved (A2) and truncated (B1) bar packages filled in to show the distribution of modeled  
185 pseudo-structures within the clinothem packages. Both packages are outlined by their defining truncation  
186 (red) and basal downlap (blue) surfaces, and internal bar surfaces (clinoforms; black lines). Bar-package  
187 measurements (reported in Figure 4 and Figure S5) are defined including package height and width, and  
188 clinoform height and width.

189

## 190 RESULTS

191 Bar-package preservation is highly variable throughout the model deposits. Globally, truncated bars  
192 are the most abundant, accounting for 58% of the bar packages mapped in the model stratigraphy. However,  
193 the proportion of cross-sectional area composed of truncated versus partially and fully preserved bars varies  
194 among cross-section locations, reaching as high as 68% preserved (partially and fully preserved packages  
195 combined) and as low as 18% preserved (i.e. 82% truncated) in some cross-sections. We find no spatial  
196 trends along the river corridor.

197 Channel widening rate and braiding intensity (eBI) along the model reach (Figure 3A-C) show no  
198 relationship with bar preservation (Figure S3 & S4). For example, cross sections at 4000 m and 4250 m  
199 have similarly low widening rates (e.g., median = 0.18 m/timestep and 0.11 m/timestep respectively; Figure  
200 3A) and comparable braiding intensities (e.g., median = 1.9 and 1.6 respectively; Figure 3B) but differ in  
201 total bar preservation by ~30% (Figure 3C). In contrast the median eBI value of the cross section at 5500  
202 m is more than double that of the section at 5750 m (2.9 vs 1.1), for comparable widening rates (0.1 vs 0.6  
203 m/timestep respectively; Figure 3A), but these sections have the similar preservation statistics between them  
204 (50% vs 59% preserved bars by area; Figure 3C).

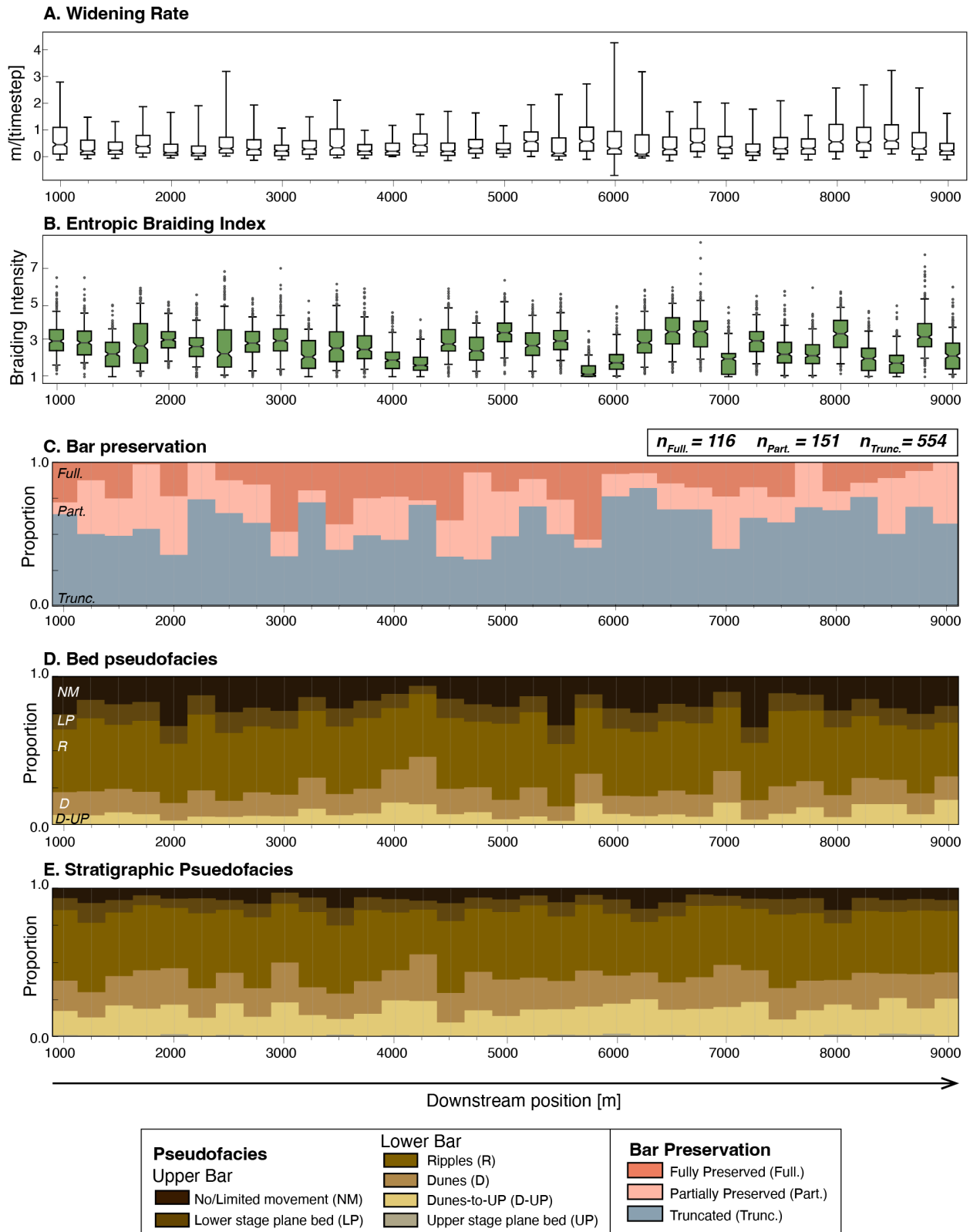
205 The aggregate distribution of pseudo-structures on the bed and within the stratigraphic cross-  
206 sections bears no correlation to Entropic Braiding Index, widening rate, or the distribution and prevalence  
207 of preserved bars in cross-sections; some cross-sections dominated by truncated bar packages exhibit  
208 relatively high fractions of low-shear-stress conditions and others reflect mostly high-shear-stress  
209 conditions (Figure 3). Similarly, although partially and fully preserved bar packages, by definition, contain  
210 upper-bar facies that represent low-shear-stress conditions, there is no evidence of cross-sections with  
211 higher bar preservation showing a higher proportion of deposits reflecting low-shear-stress flow conditions  
212 (Figure 3). Overall, the stratigraphic cross-sections—relative to the time-integrated bed average flow  
213 conditions observed on the bed throughout the model run—are skewed toward high-shear-stress deposits

214 (by cross-sectional area; Figure 3D, 3E). Bed conditions reflecting little sediment movement (No  
215 Movement and Lower-Stage-Plane-Bedding, Figure 3) are underrepresented in stratigraphic cross-sections  
216 by approximately 40% relative to their occurrence throughout the model run, and high-shear-stress  
217 conditions are overrepresented in cross-sections relative to their presence on the bed (dunes by 35% and  
218 upper-stage-plane bed by a factor of 2 relative to their occurrence on the model bed; Table S3.1).

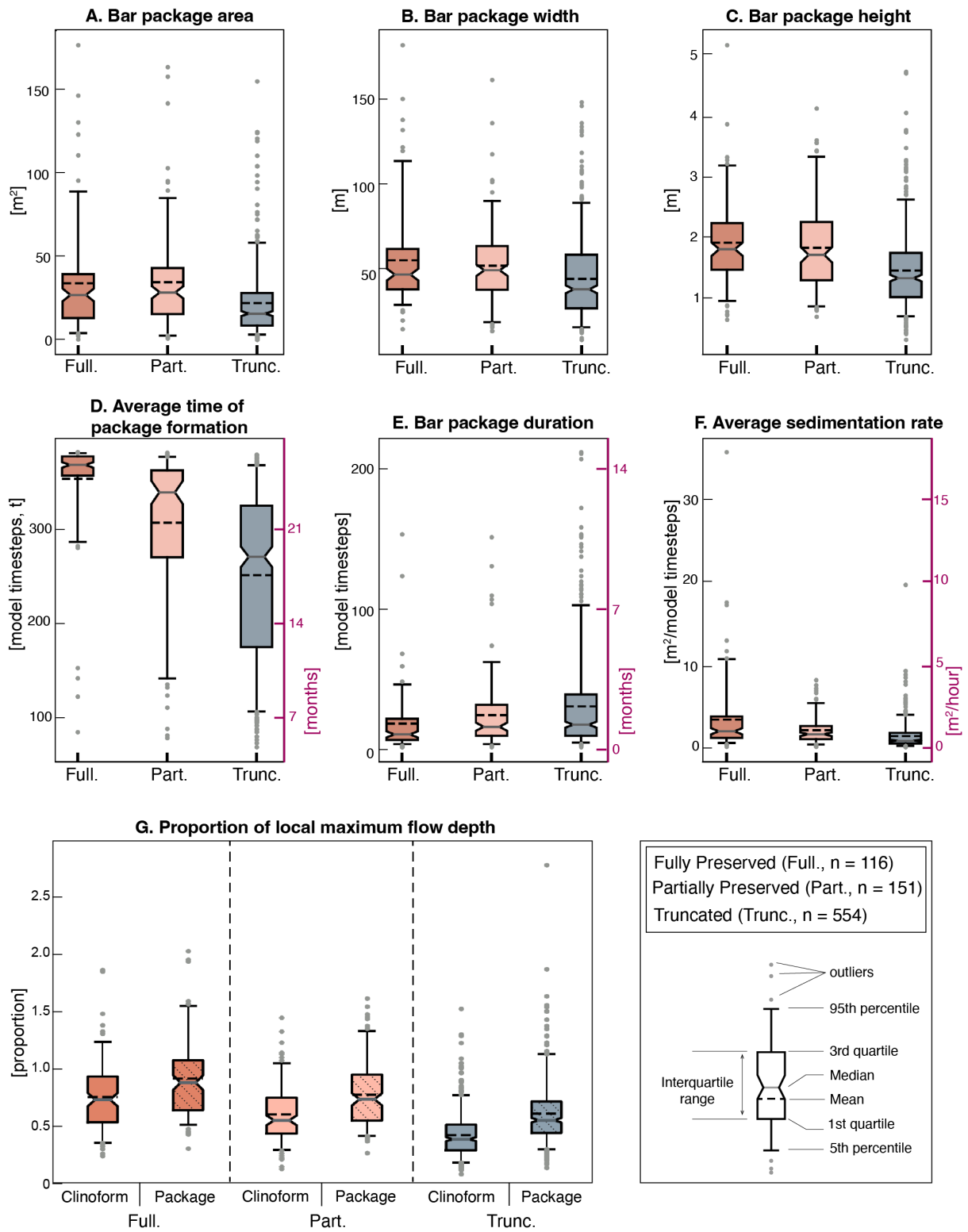
219 Fully and partially preserved packages have larger areas, widths, and heights than most truncated  
220 packages (measurements exemplified in Figure 2C; Figure 4A-C); this pattern is also reflected in individual  
221 clinothem geometries (Figure 2C, Figure S5). Additionally, fully preserved packages are the youngest  
222 packages in the mapped model stratigraphy (Figure 4D, 4E). Fully preserved bar packages that are older  
223 than 100 model timesteps represent bar packages that have persisted in the channel for longer than the  
224 average bar turnover time (Figure S2). Partially preserved and truncated bar packages have a larger spread  
225 of ages in the record (Figure 4E), and the average sedimentation rates in fully preserved packages are higher  
226 than in partially preserved and truncated packages (Figure 4F).

227 Fully preserved bar packages scale with formative channel-thread geometry at their time of  
228 deposition (Figure 4G). Both the height of preserved clinothem and bar packages scale with the local  
229 maximum flow depth for fully and partially preserved deposits. Across all preservation categories, the  
230 maximum height of bar packages is generally greater than the height of the largest clinof orm within the  
231 package, and package height scales with a greater proportion of the formative maximum flow depth  
232 associated with bar deposition than the clinof orm height. On average, the heights of partially preserved and  
233 fully preserved bar packages represent 75% and 90% of the formative flow depth, where the average  
234 truncated package represents only 57% of the local maximum flow depth during the time of bar formation.  
235 We see no evidence of preservation bias based on initial bar size, with bar packages across all preservation  
236 categories spanning the range of formative flow depths in the model (Figure S5-G).

237



239 Figure 3: Distribution of (A) channel-belt widening, and (B) Entropic Braiding Index at each mapped  
240 cross-section location (250 m apart) from t= 80 to end of model run. (C) Proportion of mapped stratigraphic  
241 cross-section area occupied by fully preserved (Full.), partially preserved (Part.) and truncated (Trunc.) bar  
242 deposits. (D) Time-integrated bed area at each cross-section location occupied by different pseudo-  
243 structures (averaged from t= 80 to the end of the model run); NM – No movement, LP – Lower stage plane  
244 bedding, R – Ripples, D – Dunes, D-UP – Dunes to Upper Stage Plane Bedding, and UP – Upper stage  
245 plane bedding). (E) Proportion of different pseudo-structures by area in each stratigraphic cross section.  
246



247

248 Figure 4: Geometric (A-C), age (D-F) and hydraulic characteristics (G) of fully, partially preserved, and

249 truncated bar packages mapped in the model domain. Secondary axes (pink) in plots D-F show model

250 timesteps converted to morphodynamic timescales (months and hours). (G) shows the distribution of  
251 clinoform and bar-package maximum relief divided by local maximum flow depth associated with the  
252 formation of the bar package for each preservation category. Inset key (lower right) describes how box and  
253 whisker plots are defined.  
254

## 255 DISCUSSION

256 Our model simulates kinematics and morphodynamics similar to those observed in active braided  
257 rivers (e.g., Rice et al., 2009; Dixon et al., 2018; Tejedor et al., 2022) with simple boundary conditions (e.g.  
258 uniform grain size, constant discharge, and no vegetation interactions and the synthetic stratigraphic  
259 architecture produced by the model reflects stratigraphic observations from braided ancient outcrops (e.g.,  
260 Miall, 1988; Gibling, 2006; Chamberlin and Hajek, 2019). While finer computation scales, a spectrum of  
261 grain sizes, and channel-floodplain coupling could provide higher resolution detail about braided river  
262 kinematics and morphodynamics, our simplified model experiment provides robust insight into the baseline  
263 behavior of unperturbed braided systems, allows for general insight into how bar deposits are preserved,  
264 and the degree to which they reflect river flow conditions.

265 Our results show that there is a spectrum of bar preservation in braided river deposits that varies  
266 spatially and is uncorrelated with time-averaged flow conditions in the channel. The shape, proportion,  
267 facies, and spatial distribution of bar preservation show no relationship to channel morphodynamics such  
268 as widening and braiding intensity. Fully and partially preserved packages generally occupy the same range  
269 of sizes and shapes as each other, and their thickness closely approximates the local maximum flow depth  
270 under which they formed. Truncated packages are generally smaller and only represent roughly half (57%)  
271 of their maximum formative flow depth. Additionally, our results highlight that the key difference between  
272 packages across preservation gradients is age, where fully preserved packages tend to be young. These results  
273 indicate that, while it may be difficult to reconstruct specific kinematics from ancient, braided river deposits,  
274 measurements of bars from braided paleochannels can be useful for 1) assessing the role of channel-belt  
275 avulsion (abandonment) on ancient landscapes, 2) comparing paleo-flow conditions across different  
276 systems, and 3) contextualizing and comparing braided river facies interpretations and paleohydraulic  
277 reconstructions from ancient deposits.

278

## 279 **Controls on bar preservation in braided river deposits**

280 In the model domain, morphodynamics, like channel-belt widening and thread migration, facilitate  
281 deposition and growth of bar packages however, preservation of these features is entirely dependent on what  
282 happens after a bar package is deposited (Figure 5). Each point on the bed experiences a unique, stochastic  
283 succession of channel kinematics that controls whether bar packages are preserved or truncated in the model  
284 stratigraphy. For example, in section A (Figure 5), packages A1 and A2 both formed during channel belt-  
285 widening events, during which bars accreted to fill lateral accommodation space created by retreating banks,  
286 but have different post-depositional histories. Package A1 was followed by a period of reworking via mobile  
287 threads, which generated a series of local deposition and erosion events. In contrast, deposition of package  
288 A2 was followed by a hiatus resulting from long-term thread abandonment (Figure 5). In contrast, section  
289 B, approximately one channel-width downstream, experienced an independent deposition-erosion history  
290 which produced a completely different stratigraphic architecture that lacks well-preserved bars (Figure 5).  
291 At this location, localized erosion and deposition events occurred across most of the channel width  
292 throughout most of the model duration; even when bars were deposited (e.g., B1), and channel activity was  
293 pervasive and dynamic enough to erode all but the youngest bar packages. Note that bar B1 was truncated  
294 by a sustained, localized erosion event, whereas bar A1 was truncated through a protracted period of  
295 alternating episodes of erosion and deposition. Furthermore, there is no trend between bar deposition or  
296 erosion and local channel braiding index or widening rate (Figure 5; Figure S3 and S4). Each cross section  
297 experiences the full, representative range of entropic braiding index (eBI) and widening rates observed  
298 throughout the model run, but there is no consistency between phases of bar formation and preservation  
299 and eBI or widening rate (Figure 5).

300 Time is a key control in the preservation of bar packages in the model stratigraphy. The youngest  
301 bars are the most likely to be preserved (Figure 4D) because they have a smaller likelihood of experiencing  
302 a channel reconfiguration that leads to erosion and reworking. This can be observed in Figure 5 where even

303 small bars (smaller, shorter runs of localized deposition) end up as preserved bar packages in both  
304 stratigraphic cross sections. In natural systems, the youngest bed configuration can be preserved through  
305 channel-belt avulsion. When a reach is abandoned, the last bars occupying the channel bed will be left  
306 intact, barring reworking and modification from intermittent flow reoccupations or other floodplain  
307 processes, and will eventually be buried by floodplain deposits from neighboring channel-belts. Stopping  
308 the model run at different timesteps yields a similar variability in preservation in one cross-section as we  
309 observe at the end of the model run among all cross-sections (Figure 3C, Figure 5). For example,  
310 preservation assessed with different stoppage (avulsion) times for the two mapped cross sections evaluated  
311 in Figure 5 shows the proportion of fully and partially preserved bars ranging from 0% to 60% with no  
312 systematic variation over time (Figure S6). This range is comparable to the range of fully and partially  
313 preserved bars among all cross-sections at the end of the model run (17% to 68%; Figure 3C), emphasizing  
314 that local preservation will be highly variable from place to place and time to time, but observing  
315 preservation over multiple cross-sections provides constraints on the background stochastic variability of  
316 deposition in the channel belt.

317         The variability in preservation across different stopping (avulsion) times in one location in space,  
318 and at the same stopping time across all cross-sections provides insight into the nuances between local  
319 sediment storage and bypass, and avulsion in braided rivers. In the model, bars on the bed turn over on  
320 daily to monthly timescales, (average ~25 days). At times in sections when the rate of bar turnover is high  
321 relative to the rate of channel morphodynamics (i.e. higher local sediment storage), bar preservation may  
322 increase. Alternatively, if the rate of bar turnover is slow relative to the rate of morphodynamics like  
323 widening and thread migration, we anticipate a decrease in bar preservation. These observed dynamics are  
324 comparable with those documented in meandering systems in which preservation is controlled by the timing  
325 of both meander bend kinematics and avulsion (Durkin et al., 2018). The interaction of bar, channel-thread  
326 and channel-belt kinematics in the model highlight how the interaction of multiple scales of processes

327 interact to influence preservation in multi-threaded systems, consistent with the concept of morphodynamic  
328 hierarchy controlling preservation in fluvial landscapes (Ganti et al., 2020). This indicates that comparing  
329 bar preservation across different systems provides an avenue for comparing the relative rates of channel-  
330 thread dynamics and avulsion timescales on ancient landscapes (e.g., Bristow and Best, 1993; Chamberlin  
331 and Hajek, 2019).

332

### 333 **Implications for reconstructing landscape conditions from braided river deposits**

334 Bar and channel deposits are important sources of information about paleoflow conditions in  
335 ancient rivers. Previous depth-scaling relationships suggest that fully preserved clinoform heights act as a  
336 proxy for paleo-flow depth (e.g., Mohrig et al., 2000; Hajek and Heller, 2012; Alexander et al., 2020). Our  
337 results corroborate that clinoforms from fully preserved bar clinoforms provide a minimum estimate of the  
338 local maximum flow depth (scaling with 75% of the formative flow depth; Figure 4) and that on average  
339 the thickness of fully preserved bar packages reflects 90% the local maximum formative channel depth  
340 associated with bar deposition (Figure 4). Even partially preserved and truncated bar packages provide scale  
341 estimates of channel depth, albeit with more uncertainty. Fully preserved bar deposits can serve as important  
342 flow-depth constraints in ancient rivers, and depending on the precision required for paleohydraulic  
343 reconstructions (e.g., Mohrig et al., 2000; Hajek and Heller, 2012; Trampusch et al., 2014; Mahon and  
344 McElroy, 2018; Lyster et al., 2021; Hartley and Owen, 2022), the scale of bar packages, regardless of  
345 preservation, can generally facilitate first-order comparisons of paleo-river size. This may be particularly  
346 useful in systems where outcrop extent and exposure limit our ability to collect these data in abundance  
347 (e.g., Ielpi et al., 2018) or in subsurface analyses in which seismic or well-log datasets limit spatial resolution  
348 (e.g., Bridge and Tye, 2000; Donselaar and Schmidt, 2005; Castelltort, 2018; Yue et al., 2019; Li et al.,  
349 2019).

350 In natural systems, channel flow conditions are reflected in the distribution of bed-material size  
351 and bedforms on the active riverbed (e.g., Southard and Boguchwal, 1990; Ashworth et al., 1992; Van Den  
352 Berg and Van Gelder, 1993). Although our pseudo-structures do not reflect specific bedform  
353 configurations, they serve as a proxy for how the spectrum of shear-stress conditions on the active bed are  
354 preserved stratigraphically, and are consistent with facies expectations of braided river deposits in ancient  
355 outcrops (e.g., Miall, 1988; Gibling, 2006; Lynds and Hajek, 2006). Deposits associated with low shear-  
356 stress conditions (regions of the channel with shallow flow depth and/or slow flow velocity) are commonly  
357 found within both preserved and truncated bars (Figure 2C) and can occupy up to 20% of some cross  
358 sections (Figure 3E). Intermediate flow conditions (“ripples” in our categorization) are present in  
359 stratigraphy in a similar proportion to the area they occupied on the bed during the model run (Figure 3D  
360 and E). High shear stress facies are overrepresented in stratigraphy relative to the area they occupy on the  
361 active channel bed (Figure 3D and 3E), likely because of greater sediment fluxes in zones of higher shear  
362 stress. The range of facies preservation in braided paleochannel deposits provides an opportunity to assess  
363 nuanced aspects of paleoflow conditions in ancient outcrops (e.g., Lynds and Hajek, 2006; Ashworth et al.,  
364 2011; Chamberlin and Hajek, 2022). Careful sampling across bar facies may provide important context for  
365 quantitative reconstructions of channel paleohydraulics (e.g., Lyster et al., 2021, 2022, 2023; Hartley and  
366 Owen, 2022; Wood et al., 2023; McLeod et al., 2023). More work is needed to fully elucidate how factors  
367 like flow variability and morphodynamic hierarchy control preservation of specific bed conditions in fluvial  
368 systems (e.g., Reesink et al., 2015; Leary and Ganti, 2020; Ganti et al., 2020; Das et al., 2022; Lyster et al.,  
369 2022), but the general consistency between mean, model bed, flow conditions and aggregate pseudo-  
370 structure abundance in stratigraphic cross-sections underscores the potential for robust comparisons of  
371 average or representative paleoflow conditions among ancient river systems.

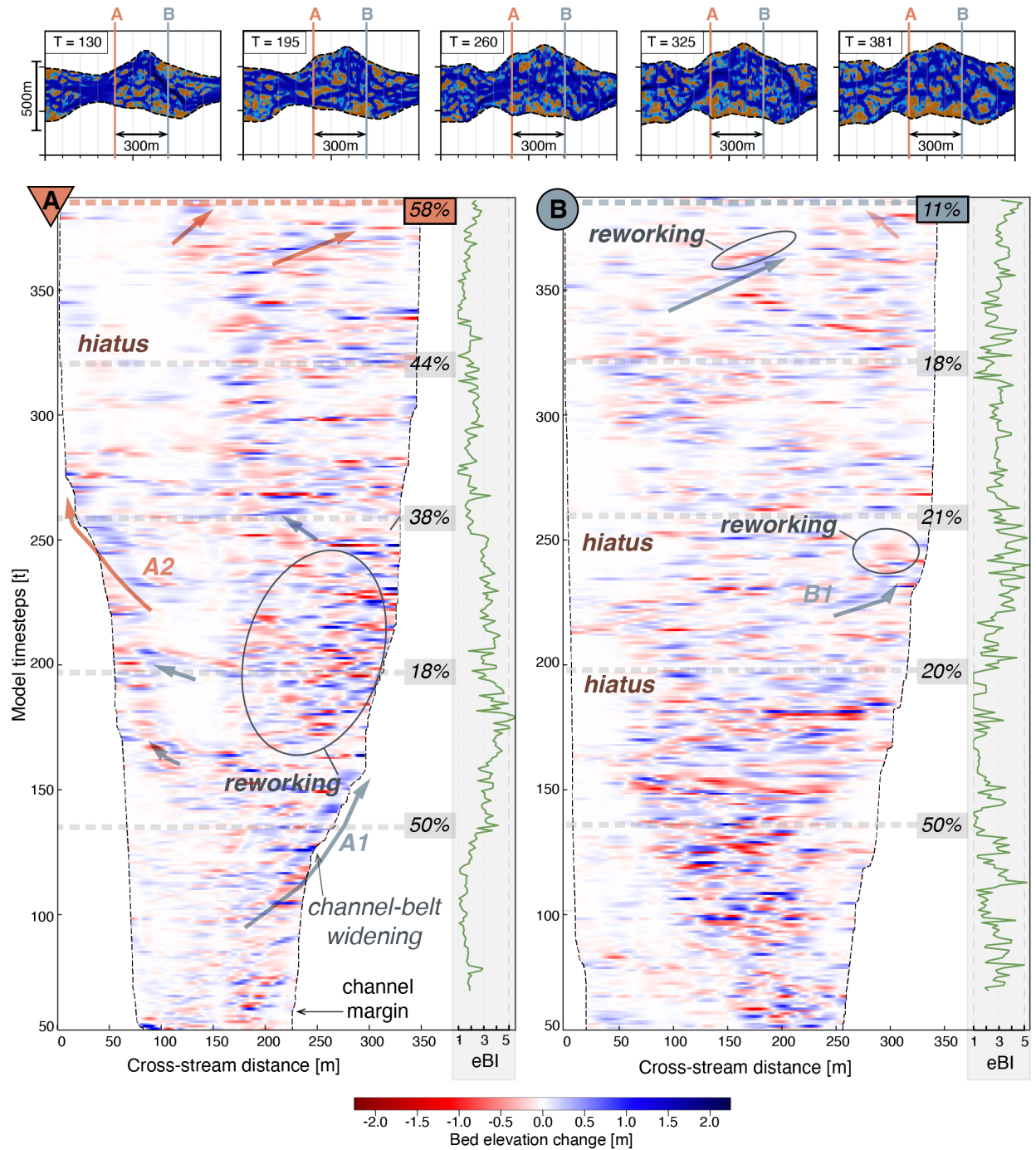
372

373 Over the course of the model run, each segment of the river experienced the full suite of channel  
374 conditions (e.g., Entropic Braiding Index, shear stress distribution, and channel widening; Figure 3)  
375 observed in the model. Although each section has its own, independent history (Figure 5), with enough  
376 time, every location in the model domain exhibited the full range of flow configurations permissible given  
377 the model setup. It follows then that in field systems, provided that sufficient cross-sections and bar  
378 packages are sampled, aggregate data collected from braided river deposits can reflect estimates of the range  
379 of flow and preservation conditions present across the formative braid belt. As an example in our model,  
380 we can reproduce the average model preservation statistics, within one standard deviation of the mean, by  
381 averaging across a random sample of cross-sections (in this case, a minimum of 3, Figure S8). Furthermore,  
382 with a minimum random sample of 30 fully preserved bar packages, we can minimize the standard deviation  
383 in measurements of the proportion of flow depth recorded by preserved bar packages (Figure S9). These  
384 statistical observations suggest that these data can be used to robustly reconstruct minimum estimates of  
385 the range of flow conditions present in the formative river system. We note that this model provides one  
386 example braided river configuration. Future efforts should explore the degree to which internal stochasticity  
387 differs among rivers with different planforms (e.g., Galeazzi et al., 2021) and across different sediment  
388 supply, discharge variability, and bank stability conditions, and how these differences might manifest in  
389 ancient deposits.

390 Collectively, insights from this study can guide how we approach the stratigraphic record. Sampling  
391 multiple outcrops and averaging over multiple exposures and sand bodies from a paleochannel network can  
392 help provide accurate pictures of ancient landscapes. However, identifying subtle and precise differences  
393 between and among systems is likely challenging given differences in outcrop quality, exposure, and extent,  
394 and, as shown in this study, the inherently large degree of variability that should be expected within deposits  
395 of a single braided channel-belt. Comparing between localities and systems across clearly defined  
396 observation scales (e.g. channel-belt, bar package, bedform) and preservation trends can be useful. For

397 example, insights from modeling in this study are consistent with preservation trends mapped in the  
398 Castlegate Formation where differences in preservation scale between localities were attributed to  
399 differences in avulsion-return time (where poorly preserved localities were associated with a relatively fast  
400 avulsion return time and well preserved localities were associated with a relatively long avulsion return time)  
401 (Chamberlin and Hajek, 2019). Field observations collected with the need for these statistical and  
402 geological consistencies in mind will help in comparing ancient systems at the bar and channel-belt scale.  
403 Furthermore, consistently mapped, and scaled field observations can contribute to broad community  
404 databases of ancient fluvial datasets that can improve analog selection for landscape reconstruction  
405 modeling, populating geologic models, and predicting and assessing subsurface connectivity in braided river  
406 aquifers and reservoirs.

Mapped stratigraphic cross-sections A and B shown in Figure 2 Panel B



407

408 Figure 5: (Top) 1 km long reach of model domain showing bed evolution at 5 timesteps during the model

409 run, and the locations of sections A (labelled with triangle) and B (labelled with circle). Stratigraphic cross-

410 sections for sections A and B shown in Figure 2 Panel B. (Bottom) Chronostratigraphic bed event

411 (erosion/deposition/hiatus) size and location diagram (Wheeler diagram) showing bed elevation change

412 throughout the model run at for Section A (left) and Section B (right) with annotations describing the  
413 thread kinematics and formation of bars A1, A2 and B1 highlighted in Figure 2 Panel B. Arrows highlight  
414 example instances of sustained deposition. Grey numbered boxes in both diagrams indicate the percentage  
415 of preserved (fully and partially) bar packages in each cross-section if the model was stopped at the timesteps  
416 shown above ( $t = 130, 195, 260, 325, 381$ ). Numbered boxes outlined in black indicate the percentage of  
417 preserved (fully and partially) packages in the final cross-sections (shown in Figure 2 Panel B) at the actual  
418 end of the model run, packages in Section A are mostly preserved while packages in Section B are primarily  
419 truncated. Green curves in the axes on the right of both bed event diagrams for section A and B show the  
420 trend in Entropic Braiding Index (eBI) at that section location throughout the model run (from the end of  
421 the model spin up period).

422 **CONCLUSIONS**

423           We used the model NAYS2DH (Jang and Shimizu, 2005; Shimizu et al., 2011; Nelson et al.,  
424 2016) to explore the relationship between channel kinematics and bar preservation in an unperturbed  
425 braided river system. Our data show that bar preservation in braided rivers is variable in both space and  
426 time and has no relationship to channel widening rate or braiding intensity as tested within the model.  
427 Ultimately, the rate of avulsion relative to the rate of bar turnover is the dominant control on bar  
428 preservation; this highlights the role of morphodynamic hierarchy in enhancing preservation of depositional  
429 elements in the stratigraphic record.

430           We find that the bar preservation and channel-belt stratigraphic architecture is product of the  
431 unique history of channel-thread movements at each location on the bed, rather than being associated with  
432 specific types of channel movements or patterns. Our observations support two final takeaways: (1) bar  
433 clinoform and package geometries provide a reasonable estimate of the local maximum flow depth during  
434 bar formation; and (2) accurately categorizing and comparing the stratigraphic architecture and paleoflow  
435 conditions of ancient, braided river deposits will benefit from consistent mapping (i.e., across defined scales  
436 of observation) and extensive sampling. This insight will strengthen efforts to disentangle the impact of  
437 flow variability on fluvial deposits and predict facies variability and textural properties in buried braided  
438 river deposits.

439

440 **ACKNOWLEDGEMENTS**

441           This work was supported by funds from the National Science Foundation granted to Hajek (EAR-  
442 1935513). We thank Harrison Martin and two anonymous reviewers for their thoughtful comments and  
443 feedback that helped to improve our manuscript Finally we would like to thank S. Lyster, R. DiBiase, D.  
444 Edmonds and R. Slingerland for insightful discussions.

445

446 **REFERENCES**

- 447 Adams, M.M., and Bhattacharya, J.P., 2005, No Change in Fluvial Style Across a Sequence Boundary,  
448 Cretaceous Blackhawk and Castlegate Formations of Central Utah, U.S.A.: *Journal of Sedimentary*  
449 *Research*, v. 75, p. 1038–1051, doi:10.2110/jsr.2005.080.
- 450 Alexander, J.S., McElroy, B.J., Huzurbazar, S., and Murr, M.L., 2020, Elevation gaps in fluvial sandbar  
451 deposition and their implications for paleodepth estimation: *Geology*, v. 48, p. 718–722,  
452 doi:10.1130/G47521.1.
- 453 Asahi, K., Shimizu, Y., Nelson, J., and Parker, G., 2013, Numerical simulation of river meandering with  
454 self-evolving banks: *Journal of Geophysical Research: Earth Surface*, v. 118, p. 2208–2229.
- 455 Ashworth, P.J., Ferguson, R.I., Ashmore, P.E., Paola, C., Powell, D.M., and Prestegards, K.L., 1992,  
456 Measurements in a Braided River chute and lobe: 2. Sorting of bed load during entrainment,  
457 transport, and deposition: *Water Resources Research*, v. 28, p. 1887–1896,  
458 doi:10.1029/92WR00702.
- 459 Ashworth, P.J., Sambrook Smith, G.H., Best, J.L., Bridge, J.S., Lane, S.N., Lunt, Ian.A., Reesink, A.J.H.,  
460 Simpson, C.J., and Thomas, R.E., 2011, Evolution and sedimentology of a channel fill in the sandy  
461 braided South Saskatchewan River and its comparison to the deposits of an adjacent compound  
462 bar: Evolution and sedimentology of a channel fill in a sandy braided river: *Sedimentology*, v. 58,  
463 p. 1860–1883, doi:10.1111/j.1365-3091.2011.01242.x.
- 464 Barefoot, E.A., Nittrouer, J.A., Foreman, B.Z., Hajek, E.A., Dickens, G.R., Baisden, T., and Toms, L.,  
465 2022, Evidence for enhanced fluvial channel mobility and fine sediment export due to precipitation  
466 seasonality during the Paleocene–Eocene thermal maximum: *Geology*, v. 50, p. 116–120,  
467 doi:10.1130/G49149.1.

468 Best, J.L., Ashworth, P.J., Bristow, C.S., and Roden, J., 2003, Three-Dimensional Sedimentary  
469 Architecture of a Large, Mid-Channel Sand Braid Bar, Jamuna River, Bangladesh: *Journal of*  
470 *Sedimentary Research*, v. 73, p. 516–530, doi:10.1306/010603730516.

471 Bradley, R.W., and Venditti, J.G., 2021, Mechanisms of Dune Growth and Decay in Rivers: *Geophysical*  
472 *Research Letters*, v. 48, p. e2021GL094572, doi:10.1029/2021GL094572.

473 Bradley, R.W., and Venditti, J.G., 2017, Reevaluating dune scaling relations: *Earth-Science Reviews*, v.  
474 165, p. 356–376, doi:10.1016/j.earscirev.2016.11.004.

475 Bridge, J.S., 1993, Description and interpretation of fluvial deposits: a critical perspective: *Sedimentology*,  
476 v. 40, p. 801–810, doi:10.1111/j.1365-3091.1993.tb01361.x.

477 Bridge, J.S., 1997, Thickness of sets of cross strata and planar strata as a function of formative bed-wave  
478 geometry and migration, and aggradation rate: *Geology*, v. 25, p. 971, doi:10.1130/0091-  
479 7613(1997)025<0971:TOSOCS>2.3.CO;2.

480 Bridge, J.S., and Lunt, I.A., 2006, Depositional Models of Braided Rivers, *in* *Braided Rivers*, John Wiley  
481 & Sons, Ltd, p. 11–50, doi:10.1002/9781444304374.ch2.

482 Bridge, J., S., and Tye, R., S., 2000, Interpreting the Dimensions of Ancient Fluvial Channel Bars,  
483 Channels, and Channel Belts from Wireline-Logs and Cores: *AAPG Bulletin*, v. 84,  
484 doi:10.1306/A9673C84-1738-11D7-8645000102C1865D.

485 Bristow, C.S., and Best, J.L., 1993, Braided rivers: perspectives and problems: Geological Society, London,  
486 Special Publications, v. 75, p. 1–11, doi:10.1144/GSL.SP.1993.075.01.01.

487 Cardenas, B.T., Lamb, M.P., Jobe, Z.R., Mohrig, D., and Swartz, J.M., 2023, Morphodynamic  
488 Preservation of Fluvial Channel Belts: *The Sedimentary Record*, v. 21, doi:10.2110/001c.66285.

489 Cardenas, B.T., Mohrig, D., Goudge, T.A., Hughes, C.M., Levy, J.S., Swanson, T., Mason, J., and Zhao,  
490 F., 2020, The anatomy of exhumed river-channel belts: Bedform to belt-scale river kinematics of  
491 the Ruby Ranch Member, Cretaceous Cedar Mountain Formation, Utah, USA (C. Fielding, Ed.):  
492 *Sedimentology*, v. 67, p. 3655–3682, doi:10.1111/sed.12765.

493 Castelltort, S., 2018, Empirical relationship between river slope and the elongation of bars in braided rivers:  
494 A potential tool for paleoslope analysis from subsurface data: *Marine and Petroleum Geology*, v.  
495 96, p. 544–550, doi:10.1016/j.marpetgeo.2018.05.008.

496 Chadwick, A.J., Steele, S., Silvestre, J., and Lamb, M.P., 2022, Effect of Sea-Level Change on River  
497 Avulsions and Stratigraphy for an Experimental Lowland Delta: *Journal of Geophysical Research:*  
498 *Earth Surface*, v. 127, p. e2021JF006422, doi:10.1029/2021JF006422.

499 Chamberlin, E.P., and Hajek, E.A., 2022, Fine-sediment Supply Can Control Fluvial Deposit  
500 Architecture: An Example From the Blackhawk Formation-Castlegate Sandstone Transition,  
501 Upper Cretaceous, Utah, USA: *The Sedimentary Record*, v. 20, doi:10.2110/001c.36334.

502 Chamberlin, E.P., and Hajek, E.A., 2015, Interpreting Paleo-Avulsion Dynamics from Multistory Sand  
503 Bodies: *Journal of Sedimentary Research*, v. 85, p. 82–94, doi:10.2110/jsr.2015.09.

504 Chamberlin, E.P., and Hajek, E.A., 2019, Using bar preservation to constrain reworking in channel-  
505 dominated fluvial stratigraphy: *Geology*, v. 47, p. 531–534, doi:10.1130/G46046.1.

506 Colombera, L., Mountney, N.P., Russell, C.E., Shiers, M.N., and McCaffrey, W.D., 2017, Geometry and  
507 compartmentalization of fluvial meander-belt reservoirs at the bar-form scale: Quantitative insight  
508 from outcrop, modern and subsurface analogues: *Marine and Petroleum Geology*, v. 82, p. 35–55,  
509 doi:10.1016/j.marpetgeo.2017.01.024.

510 Das, D., Ganti, V., Bradley, R., Venditti, J., Reesink, A., and Parsons, D.R., 2022, The Influence of  
511 Transport Stage on Preserved Fluvial Cross Strata: *Geophysical Research Letters*, v. 49, p.  
512 e2022GL099808, doi:10.1029/2022GL099808.

513 Dixon, S.J., Sambrook Smith, G.H., Best, J.L., Nicholas, A.P., Bull, J.M., Vardy, M.E., Sarker, M.H.,  
514 and Goodbred, S., 2018, The planform mobility of river channel confluences: Insights from analysis  
515 of remotely sensed imagery: *Earth-Science Reviews*, v. 176, p. 1–18,  
516 doi:10.1016/j.earscirev.2017.09.009.

517 Donselaar, M.E., and Schmidt, J.M., 2005, Integration of outcrop and borehole image logs for high-  
518 resolution facies interpretation: example from a fluvial fan in the Ebro Basin, Spain:  
519 *Sedimentology*, v. 52, p. 1021–1042, doi:10.1111/j.1365-3091.2005.00737.x.

520 Durkin, P.R., Boyd, R.L., Hubbard, S.M., Shultz, A.W., and Blum, M.D., 2017, Three-Dimensional  
521 Reconstruction of Meander-Belt Evolution, Cretaceous McMurray Formation, Alberta Foreland  
522 Basin, Canada: *Journal of Sedimentary Research*, v. 87, p. 1075–1099, doi:10.2110/jsr.2017.59.

523 Durkin, P.R., Hubbard, S.M., Holbrook, J., and Boyd, R., 2018, Evolution of fluvial meander-belt deposits  
524 and implications for the completeness of the stratigraphic record: *GSA Bulletin*, v. 130, p. 721–  
525 739, doi:10.1130/B31699.1.

526 Fielding, C.R., 2022, *Sedimentology and Stratigraphy of Large River Deposits: Recognition and*  
527 *Preservation Potential in the Rock Record*, in *Large Rivers*, John Wiley & Sons, Ltd, p. 146–170,  
528 doi:10.1002/9781119412632.ch7.

529 Fielding, C.R., Alexander, J., and Allen, J.P., 2018, The role of discharge variability in the formation and  
530 preservation of alluvial sediment bodies: *Sedimentary Geology*, v. 365, p. 1–20,  
531 doi:10.1016/j.sedgeo.2017.12.022.

532 Foreman, B.Z., 2014, Climate-driven generation of a fluvial sheet sand body at the Paleocene-Eocene  
533 boundary in north-west Wyoming (USA): *Basin Research*, v. 26, p. 225–241,  
534 doi:10.1111/bre.12027.

535 Foreman, B.Z., Heller, P.L., and Clementz, M.T., 2012, Fluvial response to abrupt global warming at the  
536 Palaeocene/Eocene boundary: *Nature*, v. 491, p. 92–95, doi:10.1038/nature11513.

537 Galeazzi, C.P., Almeida, R.P., and do Prado, A.H., 2021, Linking rivers to the rock record: Channel  
538 patterns and paleocurrent circular variance: *Geology*, v. 49, p. 1402–1407, doi:10.1130/G49121.1.

539 Ganti, V., Hajek, E.A., Leary, K., Straub, K.M., and Paola, C., 2020, Morphodynamic Hierarchy and the  
540 Fabric of the Sedimentary Record: *Geophysical Research Letters*, v. 47,  
541 doi:10.1029/2020GL087921.

542 Ganti, V., Paola, C., and Fofoula-Georgiou, E., 2013, Kinematic controls on the geometry of the  
543 preserved cross sets. *Journal of Geophysical Research: Earth Surface*, v. 118, p. 1296–1307,  
544 doi:10.1002/jgrf.20094.

545 Germanoski, D., and Schumm, S.A., 1993, Changes in Braided River Morphology Resulting from  
546 Aggradation and Degradation: *The Journal of Geology*, v. 101, p. 451–466.

547 Ghinassi, M., and Moody, J., 2021, Reconstruction of an extreme flood hydrograph and morphodynamics  
548 of a meander bend in a high-peak discharge variability river (Powder River, USA): *Sedimentology*,  
549 v. 68, p. 3549–3576, doi:10.1111/sed.12911.

550 Ghosh, S., Mandal, P., and Bera, B., 2023, Dynamics of channel bar morphology on multi-decadal  
551 timescales in a braided river within Himalayan foreland basin, India: *Journal of Earth System*  
552 *Science*, v. 132, p. 168, doi:10.1007/s12040-023-02187-x.

553 Gibling, M.R., 2006, Width and Thickness of Fluvial Channel Bodies and Valley Fills in the Geological  
554 Record: A Literature Compilation and Classification: *Journal of Sedimentary Research*, v. 76, p.  
555 731–770, doi:10.2110/jsr.2006.060.

556 Guo, W., Dong, C., Lin, C., Zhang, T., Zhao, Z., and Li, J., 2022, 3D Sedimentary Architecture of Sandy  
557 Braided River, Based on Outcrop, Unmanned Aerial Vehicle and Ground Penetrating Radar Data:  
558 *Minerals*, v. 12, p. 739, doi:10.3390/min12060739.

559 Hajek, E.A., and Heller, P.L., 2012, Flow-Depth Scaling In Alluvial Architecture and Nonmarine  
560 Sequence Stratigraphy: Example from the Castlegate Sandstone, Central Utah, U.S.A: *Journal of*  
561 *Sedimentary Research*, v. 82, p. 121–130, doi:10.2110/jsr.2012.8.

562 Hajek, E.A., Huzurbazar, S.V., Mohrig, D., Lynds, R.M., and Heller, P.L., 2010, Statistical  
563 Characterization of Grain-Size Distributions in Sandy Fluvial Systems: *Journal of Sedimentary*  
564 *Research*, v. 80, p. 184–192, doi:10.2110/jsr.2010.020.

565 Hartley, A.J., and Owen, A., 2022, Paleohydraulic analysis of an ancient distributive fluvial system: *Journal*  
566 *of Sedimentary Research*, v. 92, p. 445–459, doi:10.2110/jsr.2021.062.

567 Hartley, A.J., Owen, A., Swan, A., Weissmann, G.S., Holzweber, B.I., Howell, J., Nichols, G., and  
568 Scuderi, L., 2015, Recognition and importance of amalgamated sandy meander belts in the  
569 continental rock record: *Geology*, v. 43, p. 679–682, doi:10.1130/G36743.1.

570 Heller, P.L., and Paola, C., 1996, Downstream changes in alluvial architecture; an exploration of controls  
571 on channel-stacking patterns: *Journal of Sedimentary Research*, v. 66, p. 297–306,  
572 doi:10.1306/D4268333-2B26-11D7-8648000102C1865D.

573 Holbrook, J., and Wanas, H., 2014, A Fulcrum Approach To Assessing Source-To-Sink Mass Balance  
574 Using Channel Paleohydrologic Parameters Derivable From Common Fluvial Data Sets With An  
575 Example From the Cretaceous of Egypt: *Journal of Sedimentary Research*, v. 84, p. 349–372,  
576 doi:10.2110/jsr.2014.29.

577

578 Ielpi, A., Ghinassi, M., Rainbird, R.H., and Ventra, D., 2018, Planform sinuosity of Proterozoic rivers, *in*  
579 *Fluvial Meanders and Their Sedimentary Products in the Rock Record*, John Wiley & Sons, Ltd,  
580 p. 81–118, doi:10.1002/9781119424437.ch4.

581 Ielpi, A., Lapôtre, M.G.A., Gibling, M.R., and Boyce, C.K., 2022, The impact of vegetation on  
582 meandering rivers: *Nature Reviews Earth & Environment*, v. 3, p. 165–178, doi:10.1038/s43017-  
583 021-00249-6.

584 Jang, C.-L., and Shimizu, Y., 2005, Numerical Simulation of Relatively Wide, Shallow Channels with  
585 Erodible Banks: *Journal of Hydraulic Engineering*, v. 131, p. 565–575, doi:10.1061/(ASCE)0733-  
586 9429(2005)131:7(565).

587 Jarriel, T., Swartz, J., and Passalacqua, P., 2021, Global rates and patterns of channel migration in river  
588 deltas: *Proceedings of the National Academy of Sciences*, v. 118, p. e2103178118,  
589 doi:10.1073/pnas.2103178118.

590 Jerolmack, D.J., and Mohrig, D., 2005, A unified model for subaqueous bed form dynamics: *Water*  
591 *Resources Research*, v. 41, doi:10.1029/2005WR004329.

592 Kleinhans, M.G., and van den Berg, J.H., 2011, River channel and bar patterns explained and predicted by  
593 an empirical and a physics-based method: *Earth Surface Processes and Landforms*, v. 36, p. 721–  
594 738, doi:10.1002/esp.2090.

595 van de Lageweg, W.I., van Dijk, W.M., Box, D., and Kleinmans, M.G., 2016a, Archimetrics: a quantitative  
596 tool to predict three-dimensional meander belt sandbody heterogeneity: *The Depositional Record*,  
597 v. 2, p. 22–46, doi:10.1002/dep2.12.

598 van de Lageweg, W.I., Schuurman, F., Cohen, K.M., van Dijk, W.M., Shimizu, Y., and Kleinmans, M.G.,  
599 2016b, Preservation of meandering river channels in uniformly aggrading channel belts:  
600 *Sedimentology*, v. 63, p. 586–608, doi:10.1111/sed.12229.

601 Le Guern, J., Rodrigues, S., Tassi, P., Cordier, F., Wintenberger, C.L., and Jugé, P., 2023, Migrating bars  
602 influence the formation and dynamics of their peers in large sandy-gravel bed rivers: *Earth Surface*  
603 *Processes and Landforms*, v. 1, p. 1–14, doi:10.1002/esp.5563.

604 Leary, K.C.P., and Ganti, V., 2020, Preserved Fluvial Cross Strata Record Bedform Disequilibrium  
605 Dynamics: *Geophysical Research Letters*, v. 47, doi:10.1029/2019GL085910.

606 Leclair, S.F., Bridge, J.S., and Wang, F.Q., 1997, Preservation of cross-strata due to migration of  
607 subaqueous dunes over aggrading and non-aggrading beds: Comparison of experimental data with  
608 theory: *Geoscience Canada*, v. 24, p. 55–66.

609 Lewis, K.D., Pranter, M.J., Reza, Z.A., and Cole, R.D., 2018, Fluvial architecture of the Burro Canyon  
610 Formation using UAV-based photogrammetry and outcrop-based modeling: implications for  
611 reservoir performance, Rattlesnake Canyon, southwestern Piceance Basin, Colorado (L.  
612 Birgenheier & H. Harper, Eds.): *The Sedimentary Record*, v. 16, p. 4–10,  
613 doi:10.2110/sedred.2018.3.4.

614 Li, W., Colombera, L., Yue, D., and Mountney, N.P., 2023, Controls on the morphology of braided rivers  
615 and braid bars: An empirical characterization of numerical models: *Sedimentology*, v. 70, p. 259–  
616 279, doi:10.1111/sed.13040.

617 Li, W., Yue, D., Wang, W., Wang, W., Wu, S., Li, J., and Chen, D., 2019, Fusing multiple frequency-  
618 decomposed seismic attributes with machine learning for thickness prediction and sedimentary  
619 facies interpretation in fluvial reservoirs: *Journal of Petroleum Science and Engineering*, v. 177, p.  
620 1087–1102, doi:10.1016/j.petrol.2019.03.017.

621 Lunt, I.A., Bridge, J.S., and Tye, R.S., 2004, A quantitative, three-dimensional depositional model of  
622 gravelly braided rivers: *Sedimentology*, v. 51, p. 377–414, doi:10.1111/j.1365-3091.2004.00627.x.

623 Lynds, R., and Hajek, E., 2006, Conceptual model for predicting mudstone dimensions in sandy braided-  
624 river reservoirs: *AAPG Bulletin*, v. 90, p. 1273–1288, doi:10.1306/03080605051.

625 Lyster, S.J., Whittaker, A.C., Farnsworth, A., and Hampson, G.J., 2023, Constraining flow and sediment  
626 transport intermittency in the geological past: *Geological Society of America Bulletin*, v. 130.

627 Lyster, S.J., Whittaker, A.C., Hajek, E.A., and Ganti, V., 2022, Field evidence for disequilibrium dynamics  
628 in preserved fluvial cross-strata: A record of discharge variability or morphodynamic hierarchy?  
629 *Earth and Planetary Science Letters*, v. 579, p. 117355, doi:10.1016/j.epsl.2021.117355.

630 Lyster, S.J., Whittaker, A.C., Hampson, G.J., Hajek, E.A., Allison, P.A., and Lathrop, B.A., 2021,  
631 Reconstructing the morphologies and hydrodynamics of ancient rivers from source to sink:  
632 Cretaceous Western Interior Basin, Utah, USA (J. Peakall, Ed.): *Sedimentology*, v. 68, p. 2854–  
633 2886, doi:10.1111/sed.12877.

634 Mahon, R.C., and McElroy, B., 2018, Indirect estimation of bedload flux from modern sand-bed rivers  
635 and ancient fluvial strata: *Geology*, v. 46, p. 579–582, doi:10.1130/G40161.1.

636 Martin, R.L., and Jerolmack, D.J., 2013, Origin of hysteresis in bed form response to unsteady flows: *Water  
637 Resources Research*, v. 49, p. 1314–1333, doi:10.1002/wrcr.20093.

638 Martin, B., Owen, A., Nichols, G.J., Hartley, A.J., and Williams, R.D., 2021, Quantifying Downstream,  
639 Vertical and Lateral Variation in Fluvial Deposits: Implications From the Huesca Distributive  
640 Fluvial System: *Frontiers in Earth Science*, v. 8, p. 564017, doi:10.3389/feart.2020.564017.

641 Martin, J., Paola, C., Abreu, V., Neal, J., and Sheets, B., 2009, Sequence stratigraphy of experimental strata  
642 under known conditions of differential subsidence and variable base level: *AAPG BULLETIN*, v.  
643 93, p. 503–533, doi:10.1306/12110808057.

644 McLaurin, B.T., and Steel, R.J., 2007, Architecture and origin of an amalgamated fluvial sheet sand, lower  
645 Castlegate Formation, Book Cliffs, Utah: *Sedimentary Geology*, v. 197, p. 291–311,  
646 doi:10.1016/j.sedgeo.2006.10.005. McLeod, J.S., Wood, J., Lyster, S.J., Valenza, J.M., Spencer,  
647 A.R.T., and Whittaker, A.C., 2023, Quantitative constraints on flood variability in the rock record:  
648 *Nature Communications*, v. 14, p. 3362, doi:10.1038/s41467-023-38967-8.

649 McMahon, W.J., and Davies, N.S., 2018, Evolution of alluvial mudrock forced by early land plants:  
650 *Science*, v. 359, p. 1022–1024, doi:10.1126/science.aan4660.

651 Miall, A. D. 1994, Reconstructing Fluvial Macroform Architecture from Two-Dimensional Outcrops:  
652 Examples from the Castlegate Sandstone, Book Cliffs, Utah: *SEPM Journal of Sedimentary*  
653 *Research*, v. Vol. 64B, doi:10.1306/D4267F78-2B26-11D7-8648000102C1865D.

654 Miall, A.D., 1988, Architectural elements and bounding surfaces in fluvial deposits: anatomy of the  
655 Kayenta formation (lower jurassic), Southwest Colorado: *Sedimentary Geology*, v. 55, p. 233–262,  
656 doi:10.1016/0037-0738(88)90133-9.

657 Miall, A.D., 1985, Architectural-Element Analysis: A New Method of Facies Analysis Applied to Fluvial  
658 Deposits: *Earth-Science Reviews*, v. 22, p. 261–308.

659 Mohrig, D., Heller, P.L., Paola, C., and Lyons, W.J., 2000, Interpreting avulsion process from ancient  
660 alluvial sequences: Guadalupe-Matarranya system (northern Spain) and Wasatch Formation  
661 (western Colorado): Geological Society of America Bulletin,

662 Myrow, P.M., Jerolmack, D.J., and Perron, J.T., 2018, Bedform Disequilibrium: Journal of Sedimentary  
663 Research, v. 88, p. 1096–1113, doi:10.2110/jsr.2018.55.

664 Nelson, J.M. et al., 2016, The international river interface cooperative: Public domain flow and  
665 morphodynamics software for education and applications: Advances in Water Resources, v. 93, p.  
666 62–74, doi:10.1016/j.advwatres.2015.09.017.

667 Nicholas, A.P. et al., 2016, The role of discharge variability in determining alluvial stratigraphy: Geology,  
668 v. 44, p. 3–6, doi:10.1130/G37215.1.

669 Owen, A., Nichols, G.J., Hartley, A.J., Weissmann, G.S., and Scuderi, L.A., 2015, Quantification of a  
670 Distributive Fluvial System: The Salt Wash DFS of the Morrison Formation, SW U.S.A.: Journal  
671 of Sedimentary Research, v. 85, p. 544–561, doi:10.2110/jsr.2015.35.

672 Paola, C., and Borgman, L., 1991, Reconstructing random topography from preserved stratification:  
673 Sedimentology, v. 38, p. 553–565, doi:10.1111/j.1365-3091.1991.tb01008.x.

674 Paola, C., Straub, K., Mohrig, D., and Reinhardt, L., 2009, The “unreasonable effectiveness” of  
675 stratigraphic and geomorphic experiments: Earth-Science Reviews, v. 97, p. 1–43,  
676 doi:10.1016/j.earscirev.2009.05.003.

677 Rahman, M.R., 2023, River dynamics – a geospatial analysis of Jamuna (Brahmaputra) River in Bangladesh  
678 during 1973–2019 using Landsat satellite remote sensing data and GIS: Environmental  
679 Monitoring and Assessment, v. 195, p. 96, doi:10.1007/s10661-022-10638-z.

680 Reesink, A.J.H., Van den Berg, J.H., Parsons, D.R., Amsler, M.L., Best, J.L., Hardy, R.J., Orfeo, O., and  
681 Szupiany, R.N., 2015, Extremes in dune preservation: Controls on the completeness of fluvial  
682 deposits: *Earth-Science Reviews*, v. 150, p. 652–665, doi:10.1016/j.earscirev.2015.09.008.

683 Rice, S.P., Church, M., Wooldridge, C.L., and Hickin, E.J., 2009, Morphology and evolution of bars in a  
684 wandering gravel-bed river; lower Fraser river, British Columbia, Canada: *Sedimentology*, v. 56,  
685 p. 709–736, doi:10.1111/j.1365-3091.2008.00994.x.

686 Sahoo, H., Gani, M.R., Gani, N.D., Hampson, G.J., Howell, J.A., Storms, J.E.A., Martinius, A.W., and  
687 Buckley, S.J., 2020, Predictable patterns in stacking and distribution of channelized fluvial sand  
688 bodies linked to channel mobility and avulsion processes: *Geology*, v. 48, p. 903–907,  
689 doi:10.1130/G47236.1.

690 Sambrook Smith, G.H., Nicholas, A.P., Best, J.L., Bull, J.M., Dixon, S.J., Goodbred, S., Sarker, M.H.,  
691 and Vardy, M.E., 2019, The sedimentology of river confluences (C. Bristow, Ed.): *Sedimentology*,  
692 v. 66, p. 391–407, doi:10.1111/sed.12504.

693 Sambrook Smith, G.H., Best, J.L., Ashworth, P.J., Lane, S.N., Parker, N.O., Lunt, I.A., Thomas, R.E.,  
694 and Simpson, C.J., 2010, Can we distinguish flood frequency and magnitude in the  
695 sedimentological record of rivers? *Geology*, v. 38, p. 579–582, doi:10.1130/G30861.1.

696 Schuurman, F., and Kleinhans, M.G., 2015, Bar dynamics and bifurcation evolution in a modelled braided  
697 sand-bed river: Bar dynamics and bifurcation evolution in a modelled braided sand-bed river: *Earth  
698 Surface Processes and Landforms*, v. 40, p. 1318–1333, doi:10.1002/esp.3722.

699 Schuurman, F., Kleinhans, M.G., and Middelkoop, H., 2016, Network response to disturbances in large  
700 sand-bed braided rivers: *Earth Surface Dynamics*, v. 4, p. 25–45, doi:10.5194/esurf-4-25-2016.

701 Sharma, N., Whittaker, A.C., Watkins, S.E., Valero, L., Vérité, J., Puigdefabregas, C., Adatte, T., Garcés,  
702 M., Guillocheau, F., and Castelltort, S., 2023, Water discharge variations control fluvial  
703 stratigraphic architecture in the Middle Eocene Escanilla formation, Spain: *Scientific Reports*, v.  
704 13, p. 6834, doi:10.1038/s41598-023-33600-6.

705 Shimizu, Y., Takebayashi, H., Inoue, T., Hamaki, M., Iwasaki, T., and Nabi, M., 2011, NAYS2DH Solver  
706 Manual:; <https://i-ric.org/en/download/nays2dh-mensual-v3/> (accessed February 2020).

707 Smith, D.G., Hubbard, S.M., Lavigne, J.R., Leckie, D.A., and Fustic, M., 2011, Stratigraphy of Counter-  
708 Point-Bar and Eddy-Accretion Deposits in Low-Energy Meander Belts of the Peace-Athabasca  
709 Delta, Northeast Alberta, Canada, *in* Davidson, S.K., Leleu, S., and North, C.P. eds., *From River  
710 to Rock Record: The preservation of fluvial sediments and their subsequent interpretation*, SEPM  
711 Society for Sedimentary Geology, v. 97, p. 0, doi:10.2110/sepmsp.097.143.

712 Southard, J.B., and Boguchwal, L.A., 1990, Bed Configurations in Steady Unidirectional Water Flows.  
713 Part 2. Synthesis of Flume Data:

714 Straub, K.M., and Wang, Y., 2013, Influence of water and sediment supply on the long-term evolution of  
715 alluvial fans and deltas: Statistical characterization of basin-filling sedimentation patterns: *Basin  
716 Filling Sedimentation Patterns: Journal of Geophysical Research: Earth Surface*, v. 118, p. 1602–  
717 1616, doi:10.1002/jgrf.20095.

718 Strong, N., Sheets, B., Hickson, T., and Paola, C., 2005, A Mass-Balance Framework for Quantifying  
719 Downstream Changes in Fluvial Architecture, *in* Blum, M.D., Marriott, S.B., and Leclair, S.F.  
720 eds., *Fluvial Sedimentology VII*, Oxford, UK, Blackwell Publishing Ltd., p. 243–253,  
721 doi:10.1002/9781444304350.ch14.

- 722 Sylvester, Z., Durkin, P.R., Hubbard, S.M., and Mohrig, D., 2021, Autogenic translation and counter  
723 point bar deposition in meandering rivers: *GSA Bulletin*, v. 133, p. 2439–2456,  
724 doi:10.1130/B35829.1.
- 725 Tejedor, A., Schwenk, J., Kleinhans, M., Limaye, A.B., Vulis, L., Carling, P., Kantz, H., and Foufoula-  
726 Georgiou, E., 2022, The Entropic Braiding Index (eBI): A Robust Metric to Account for the  
727 Diversity of Channel Scales in Multi-Thread Rivers: *Geophysical Research Letters*, v. 49, p.  
728 e2022GL099681, doi:10.1029/2022GL099681.
- 729 Trampush, S.M., Huzurbazar, S., and McElroy, B., 2014, Empirical assessment of theory for bankfull  
730 characteristics of alluvial channels: *Water Resources Research*, v. 50, p. 9211–9220,  
731 doi:10.1002/2014WR015597.
- 732 Van Den Berg, J.H., and Van Gelder, A., 1993, A New Bedform Stability Diagram, with Emphasis on the  
733 Transition of Ripples to Plane Bed in Flows over Fine Sand and Silt, *in* Marzo, M. and  
734 Puigdefbregas, C. eds., *Alluvial Sedimentation*, Oxford, UK, Blackwell Publishing Ltd., p. 11–21,  
735 doi:10.1002/9781444303995.ch2.
- 736 Wickert, A.D., Martin, J.M., Tal, M., Kim, W., Sheets, B., and Paola, C., 2013, River channel lateral  
737 mobility: metrics, time scales, and controls: *Journal of Geophysical Research: Earth Surface*, v. 118,  
738 p. 396–412, doi:10.1029/2012JF002386.
- 739 Wintenberger, C.L., Rodrigues, S., Claude, N., Jugé, P., Bréhéret, J.-G., and Villar, M., 2015, Dynamics  
740 of nonmigrating mid-channel bar and superimposed dunes in a sandy-gravelly river (Loire River,  
741 France): *Geomorphology*, v. 248, p. 185–204, doi:10.1016/j.geomorph.2015.07.032.

742 Wood, J., McLeod, J.S., Lyster, S.J., and Whittaker, A.C., 2023, Rivers of the Variscan Foreland: fluvial  
743 morphodynamics in the Pennant Formation of South Wales, UK: *Journal of the Geological*  
744 *Society*, v. 180, p. jgs2022- 048, doi:10.1144/jgs2022-048.

745 Yue, D., Li, W., Wang, W., Hu, G., Qiao, H., Hu, J., Zhang, M., and Wang, W., 2019, Fused spectral-  
746 decomposition seismic attributes and forward seismic modelling to predict sand bodies in  
747 meandering fluvial reservoirs: *Marine and Petroleum Geology*, v. 99, p. 27–44,  
748 doi:10.1016/j.marpetgeo.2018.09.031.

749